Anisotropic fluctuations in turbulent shear flows

Anisotropic fluctuations in turbulent shear flows

Boris Jacob
Dipartimento di Meccanica e Aeronautica, Università di Roma "La Sapienza," via Eudossiana 18, 00184 Roma, Italy

Luca Biferale
Dipartimento di Fisica and INFM Università "Tor Vergata," via della Ricerca Scientifica 1, 00133 Roma, Italy

Gaetano Iuso
DIAS, Politecnico di Torino, corso Duca degli Abruzzi 24, 10129 Torino, Italy

Carlo Massimo Casciola
Dipartimento di Meccanica e Aeronautica, Università di Roma "La Sapienza," via Eudossiana 18, 00184 Roma, Italy

(Received 12 February 2004; accepted 13 July 2004; published online 6 October 2004)

An experimental analysis of small-scale anisotropic fluctuations has been performed in two different flows in order to assess possible universal features of shear dominated turbulence, such as the decay rate of anisotropy at small scales and the recovery of isotropy. The two data sets—a homogeneous shear flow and a turbulent boundary layer—are characterized by turbulent Reynolds numbers in the range $\mathrm{Re}_\lambda = 230-330$. The measurements in the logarithmic region of the turbulent boundary layer extend from $y^+ = 90$ up to $y^+ = 350$. The explicit use of the Taylor hypothesis is avoided by resorting to two-point measurements, with separation in the spanwise direction, z. Streamwise (u) and wall-normal (v) velocity components are simultaneously measured in both positions by means of cross-wire probes. This procedure allows the construction of the mixed transverse structure functions, here addressed up to order 6. According to the SO(3) formalism, the observables we selected are free of any isotropic contribution, thus allowing a direct measurement of the fully anisotropic component of the field. The results are consistent with the "exponent-only" scenario for universality, i.e., all experimental data can be fitted by fixing the same set of anisotropic scaling exponents by changing only the prefactors, for different shear intensities and boundary conditions. © *2004 American Institute of Physics*. [DOI: 10.1063/1.1789546]

I. INTRODUCTION

Statistical theory of turbulence is often focused on homogeneous and isotropic flows.[1] Experimentally, however, we know that isotropy holds only approximately, with different degrees of justification, depending on the geometry of the boundaries and on the driving mechanism. Therefore, a realistic description of turbulence cannot ignore anisotropic and nonhomogeneous effects, especially in regions close to the boundaries, and/or at scales close to the integral scale, L_0, where the injection mechanism can strongly affect velocity fluctuations. The interest in quantifying anisotropic and nonhomogeneous effects is also linked to the important issue of "recovery of isotropy," i.e., the problem of "small-scale universality." Surprisingly enough, recent experimental and numerical works[2–7] have detected the survival of anisotropic turbulent fluctuations down to the Kolmogorov scale, η. These findings have stimulated a lot of further experimental, numerical, and theoretical work focused on developing proper analytical tools[8] and extending the available experimental/numerical data sets.[2–7,9–13] Much progress has been achieved. For example, the so-called puzzle of "persistence of anisotropies" in small-scale—high Reynolds numbers—shear flows, has been recently understood as the effect of strong anomalous anisotropic fluctuations.[7,13] The attention is mainly focused on correlation functions based on gradients (to probe Reynolds number dependency) or on the projections on isotropic/anisotropic sectors of multipoints velocity correlation functions, $S^{\{\alpha\}}(\mathbf{r}_1,\ldots,\mathbf{r}_n) \equiv \langle v_{\alpha_1}(\mathbf{r}_1)\ldots v_{\alpha_n}(\mathbf{r}_n)\rangle$, where we use $\{\alpha\}$ as a shorthand notation for the ensemble of indices $\alpha_1,\ldots,\alpha_n$. When all spatial separations, $\mathbf{r}_1\ldots\mathbf{r}_n$, are in the inertial range, $\eta \ll |\mathbf{r}_i - \mathbf{r}_j| \sim r \ll L_0$, one expects the existence of power law behavior under a uniform space dilation: $S^{\{\alpha\}}(\lambda\mathbf{r}_1,\ldots,\lambda\mathbf{r}_n) = \lambda^{\xi(n)} S^{\{\alpha\}}(\mathbf{r}_1,\ldots,\mathbf{r}_n)$. Most of the recent works in anisotropic turbulence concentrated on determining the values of the exponent, $\xi(n)$, as a function of the order of the correlation function, n, and of its anisotropic properties. Indeed, an important step forward was taken by realizing that different projections of the multipoint correlation functions on different irreducible representation of the group of rotation, SO(3), possess different scaling properties. The idea is to decompose any correlation function in a complete basis of eigenfunctions with defined properties under rotations. Each eigenfunction identifies a specific anisotropic sector with total angular momentum, j, and its projection, m, on a given axis. It is believed that the scaling properties of the projections on different sectors possess different scaling exponents, $\xi_j(n)$. Exponents for the fully isotropic sectors are labeled by

$j=0$ while more and more anisotropic fluctuations are measured by higher and higher values of j.[8,10]

The higher-than-expected presence of small-scale anisotropic fluctuations raises questions about their universal or nonuniversal origins. In other words, we wish to check if *all* flows possess the same, or similar, anisotropic small-scale fluctuations independently of their large-scale behavior. Of course, full universality cannot be expected, and one is tempted to look for an "exponent-only" scenario, i.e., only the scaling exponents, $\xi_j(n)$, pertaining to each different anisotropic sector are universal, while the overall correlation functions intensities are not. This hypothesis is inspired by both theoretical reasons[8,14] and similarities with what has been observed for isotropic fluctuations.[15]

To date, there are a few experimental and numerical data sets where universality of anisotropic fluctuations has been probed. These include detailed experimental investigations of anisotropic small-scale fluctuations both in laboratory flows[3,4,16] and in the atmospheric boundary layer.[10–12] On the numerical side, only a few direct numerical simulations (DNS) in highly anisotropic flows have been performed with the aim to explicitly test the small-scale properties of anisotropic fluctuations.[6,9,13,17,18] The situation is not fully resolved yet. On the experimental side, due to the difficulty in measuring multipoint multicomponent velocity statistics, one can access only the $j=2$ sector. On the other hand, DNS can properly disentangle fluctuations of all sectors, but due to limitations in the Reynolds numbers, only results in the $j=4$ and $j=6$ sectors have been obtained with some accuracy. The $j=2$ sector in the numerical works[6,17] was not measurable due to strong finite Reynolds number effects. Results from different experiments, with different geometries and different large scale structures, are in fairly good agreement concerning the $j=2$ sector up to the moment $n=6$. Putting together all results of numerics and experiments one recovers a scenario for anisotropic fluctuations consistent (not in contradiction) with the exponent-only picture of universality. Still, more tests in both experiments and numerics are needed.

The aim of this paper is to present a systematic assessment of anisotropic fluctuations in shear flows by changing both the experimental setup and the shear intensity. In particular, we have measured small-scale turbulent properties in a homogeneous shear flow (HS) and in a turbulent boundary layer (TBL). In the approach presented here the SO(3) machinery is applied to data from two cross-wire probes at varying separation—see, e.g., Ref. 3, for an example of multiprobe acquisitions in a related context. In this way two velocity components are simultaneously acquired at two locations in order to extract information at different scales with no need for Taylor hypothesis of frozen turbulence. These kinds of multipoint multicomponent measurements are necessary in order to disentangle contributions from isotropic and anisotropic fluctuations and from among different kinds of anisotropic fluctuations.

Our results support the exponent-only scenario. We found good qualitative and quantitative agreement of the anisotropic scaling exponents in both HS and TBL flows. Moreover, our results are in agreement with the previously measured values in different experiments with different Reynolds numbers and different shear intensities.

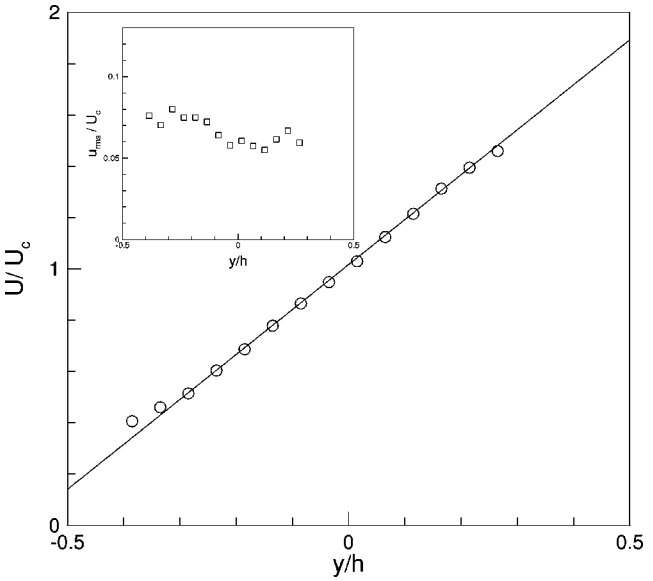

FIG. 1. Homogeneous shear flow: Mean velocity profile as a function of the nondimensional coordinate in the mean gradient direction, y/h. In the inset, the normalized streamwise turbulent intensity $u_{\rm rms}$. Velocities are normalized in terms of the centerline velocity, $U_c=10.2\ {\rm m\,s^{-1}}$, while the test section height is $h=0.9$ m.

The paper is organized as follows. In Sec. II we present the details of the two experimental apparatus including some typical large-scale measurements to validate the laboratory setup. In Sec. III we present the scaling properties for both HS and TBL flows. Conclusions follow in Sec. IV.

II. EXPERIMENTAL SETUP

The data we are going to discuss concern two different experiments, both conducted in the $1.30\ {\rm m}\times 0.90\ {\rm m}$ test section of a 7 m long open-return wind tunnel. The first data set has been obtained in a nominally HS flow, characterized by a constant velocity gradient. The second one refers to measurements performed in the logarithmic region of a zero pressure gradient TBL.

A. Homogeneous shear flow

The setup of the homogeneous shear flow is based on the original idea proposed in Ref. 19, see also Ref. 20. The mean shear is generated with a device consisting of a series of 15 adjacent small channels, equipped with screens of different solidity to produce suitable pressure drops. The channels are followed by flow straighteners in a way so as to generate a linear mean velocity profile $U(y)$ sufficiently downstream. The data shown in Fig. 1 correspond to a measurement $\approx$4.8 m downstream the apparatus, where the flow is already well developed. Concerning fluctuations, the deviations from the ideal constant profile of the streamwise turbulence intensity $u_{\rm rms}(y)=\langle(u-U)^2\rangle^{1/2}$ are comparable with those observed in similar setups.[2] In particular, they are of the order of 7% in the central part of the test section where the data to be discussed below were measured. At this location ($x/h\sim 5$,

TABLE I. Basic parameters for the homogeneous shear flow. Symbols are defined as follows: The rms fluctuation intensity in the streamwise direction is $u_{rms}=\langle(u-U)^2\rangle^{1/2}$, and analogous definitions apply for v_{rms} and w_{rms}. $\rho_{uv}=\langle uv\rangle/(u_{rms}v_{rms})$ is the correlation coefficient, ϵ is the energy dissipation rate evaluated in terms of the one-dimensional spectrum $E_{11}(\kappa_1)$: $15\nu\int\kappa_1^2E_{11}(\kappa_1)d\kappa_1$. ℓ_T is the transverse integral length scale, $\int\langle u(x,y,z)u(x,y,z+r_z)\rangle dr_z/u_{rms}^2$ and $\eta=(\nu^3/\epsilon)^{1/4}$ is the Kolmogorov scale. The Taylor–Reynolds number is $\mathrm{Re}_\lambda=\lambda u_{rms}/\nu$, where the Taylor scale follows from $\sqrt{15\nu u_{rms}^2/\epsilon}$ and the shear parameter is $S^*=\sqrt{Su_{rms}^2/\epsilon}$.

u_{rms} (m s^{-1})	v_{rms} (m s^{-1})	ρ_{uv}	ϵ (m^2 s^{-3})	ℓ_T (mm)	η (mm)	Re_λ	S^*
0.43	0.31	–0.3	0.6	53	0.28	250	4.9

where h is the tunnel height) the correlation coefficient ρ_{uv} has already attained its equilibrium value, about –0.3, consistent with results found in similar configurations,[2] which are located in the range $[-0.52,-0.25]$. Finally, we note that the dimensionless shear rate $S^*\simeq 5$ (Table I) is a factor 2 smaller than achieved in the logarithmic part of the turbulent boundary layer (Table II).

B. Boundary layer

The boundary layer develops on the smooth surface of the lower wall of the tunnel, where a nominal zero pressure gradient is achieved by adjusting the upper wall. The measurements have been performed on the centerline of the test section, 6.0 m downstream from the tripping device at the end of the contraction. With an external velocity U_∞ of 11.5 m/s, the thickness of the boundary layer at this location is approximately $\delta\simeq 40$ mm, while the Reynolds number based on the momentum thickness Re_θ is ≈ 6500, well within the range pertaining to a fully developed turbulent boundary layer. The friction velocity, $u_\tau=\sqrt{\tau_w/\rho}$ (with τ_w the average shear stress at the wall and ρ the constant density) estimated from the mean velocity profile with a Clauser chart, is $u_\tau=0.43$ m s^{-1}, in good agreement ($\pm 8\%$) with a direct measurement by means of a Preston tube. The streamwise mean velocity $U(y)$ and the fluctuation intensity $u_{rms}(y)$ profiles are displayed in Fig. 2. Both curves show that the flow complies with the requirements of a fully developed turbulent boundary layer.

C. Data acquisition

The instrumentation consists essentially of two subminiature X probes, mounted on streamlined supports in order to minimize interference effects, and separated in the transverse direction (see Fig. 3). The wires are 2.5 μm in diameter, 0.5 mm in effective length and in separation, oriented at $\pm 45°$ with respect to the streamwise direction. They are operated at an overheat ratio 1.9. Single component subminiature probes (diameter 2.5 μm, length to diameter ratio equal to 200 to minimize conduction losses) have also been used to measure the velocity profiles. The signals from the two X wires are simultaneously digitized at 21 kHz with a 16-bit data-acquisition board, after being low-pass filtered at the Nyquist frequency and suitably amplified to achieve a good signal-to-noise ratio. The frequency response of the hot wires, measured in the free stream at a reference velocity $U=6$ ms^{-1}, is larger than 15 kHz. In this way, the resolution needed to analyze the small-scale behavior down to the Kolmogorov scale η—typically of the order of 0.1–0.2 mm—is guaranteed. The X wires are calibrated *in situ* against a Pitot tube. The mapping between the output voltages and the components of the velocity (u,v) is obtained by varying both the reference velocities and the orientation of the probe with respect to the flow (see, e.g., Ref. 21). The calibration was repeated at the end of each set of measurements, to check that no voltage drift had occurred.

As for the length of the signals, they consist typically of $4-8\times 10^6$ samples, corresponding roughly to 2×10^4 eddy turnover times for both flows. Convergence of the statistics has been checked up to the sixth moment.

III. RESULTS

Scaling properties of anisotropic fluctuations are traditionally addressed through objects that are identically zero in homogeneous isotropic conditions. Typically, the study has been confined to the cospectra.[22] Recently a new extended set of observables has been proposed in the context of the SO(3) decomposition. The idea is to exploit the expansion of any generic statistical observable in terms of a suitable eigenbasis with a well characterized behavior under rotations,[8] see also Refs. 4 and 11 for successive applications. Let us focus, for instance, on the generic element in the space of second order correlation tensors

TABLE II. Basic parameters for the boundary layer. For definitions see caption of Table I.

y^+	u_{rms} (m s^{-1})	v_{rms} (m s^{-1})	ρ_{uv}	ϵ (m^2 s^{-3})	ℓ_T (mm)	η (mm)	Re_λ	S^*
350	0.94	0.45	–0.37	7.1	12.2	0.15	330	12.1
240	1.01	0.47	–0.39	11.0	8.6	0.13	300	12.8
140	1.06	0.48	–0.38	13.7	7.1	0.125	250	14.2
90	1.07	0.46	–0.36	23.0	6.6	0.11	230	15.9

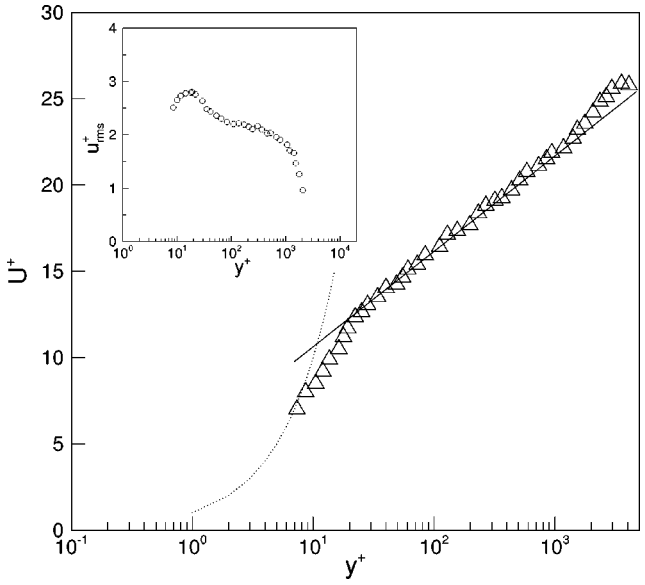

FIG. 2. Turbulent boundary layer: Mean velocity profile U^+ vs wall normal distance y^+ in wall units. The dotted line corresponds to the linear behavior $U^+=y^+$, while the solid line indicates the log-law: $U^+=(1/\kappa)\ln y^+ + B$, with $\kappa=0.41$ and $B=5.1$. The inset shows the streamwise turbulent fluctuation $u^+_{\rm rms}$. Wall units are defined in terms of the friction velocity and the kinematic viscosity ν, thus $U^+=U/u_\tau$, $u^+_{\rm rms}=u_{\rm rms}/u_\tau$, and $y^+=u_\tau y/\nu$.

$$S_{\alpha_1\alpha_2}(\mathbf{r})=\left\langle \delta v_{\alpha_1}(\mathbf{r})\,\delta v_{\alpha_2}(\mathbf{r})\right\rangle, \tag{1}$$

where $\delta v_\alpha(\mathbf{r})$ denotes the αth component of the velocity increment at two points separated by the vector $\mathbf{r}$, $\delta v_\alpha(\mathbf{r}) \equiv v_\alpha(\boldsymbol{x}+\boldsymbol{r})-v_\alpha(\boldsymbol{x})$. The appropriate SO(3) decomposition of Eq. (1) reads[8]

$$S_{\alpha_1\alpha_2}(\mathbf{r})=\sum_{j=0}^{\infty}\sum_{m=-j}^{+j}\sum_{q=1}^{p(j)} S^{(2)}_{jmq}(r)B^{jmq}_{\alpha_1\alpha_2}(\hat{\mathbf{r}}). \tag{2}$$

Here the index j denotes a sector, to be understood as a subspace invariant with respect to rotations, $B^{jqm}_{\alpha_1\alpha_2}$ denotes the appropriate basis function,[8] which depends on the unit vector $\hat{\mathbf{r}}$ and $p(j)$ counts the number of irreducible representations. In particular, $j=0$ labels the isotropic sector, while sectors of increasing anisotropy correspond to higher and higher j's. Information on the dynamics of the system is now captured by the coefficients $S^{(2)}_{jmq}$ which depend only on distance r.

The invariance under rotations of the inertial terms of the Navier–Stokes equations suggests that small-scale statistics depends only on the sector under consideration. For Reynolds large enough, scaling laws of the projection are, therefore, expected in the form

$$S^{(2)}_{jmq}(r)\sim r^{\xi_j(2)},$$

where the scaling exponent explicitly depends on the sector, j, while the argument (2) reminds that we are presently dealing with a second order tensor. The machinery can be easily extended to structure functions of any order n,

$$S_{\alpha_1\ldots\alpha_n}(\mathbf{r})=\left\langle \delta v_{\alpha_1}(\mathbf{r})\ldots\delta v_{\alpha_n}(\mathbf{r})\right\rangle,$$

whose projection on the proper SO(3) basis will possess a scaling behavior

$$S^{(n)}_{jmq}(r)\sim r^{\xi_j(n)}.$$

In this context, the recovery of isotropy at smaller and smaller scales corresponds to the existence of a hierarchy of exponents $\xi_{j=0}(n)<\xi_j(n)$.[7,8]

Scaling laws for the anisotropic sectors have been recently addressed by using different DNS databases.[6,7,18] From the experimental point of view, the evaluation of the proper SO(3) components of a given correlation tensor is hampered by the limited information on its spatial dependence. In the latter case, the simplest approach is to take a selection of tensorial components such as to cancel out the isotropic contribution in the expansion (2). For example, the component $S_{12}(\mathbf{r})$ in the direction $\mathbf{r}=(0,0,r_3)$ vanishes in a purely isotropic ensemble. Still, in principle all anisotropic sectors may influence its behavior. One may follow two possibilities. Either one may extract the whole anisotropic spectrum by making a multiparameter fit in all sectors[10] or may assume, as done in the present paper, that at scales small enough the correlation function is dominated by the leading anisotropic contribution.[4,11] Considering that in the geometrical setup of our interest $j=1$ sector is absent by symmetry, one assumes that in the small-scale limit (at high Reynolds numbers) the leading behavior of Eq. (2) is given by the $j=2$ sector

$$S_{\alpha_1\alpha_2}(\mathbf{r})\sim\sum_{m=-2}^{+2}\sum_{q=1}^{p(2)} S^{(2)}_{2mq}(r)B^{2mq}_{\alpha_1\alpha_2}(\hat{\mathbf{r}}).$$

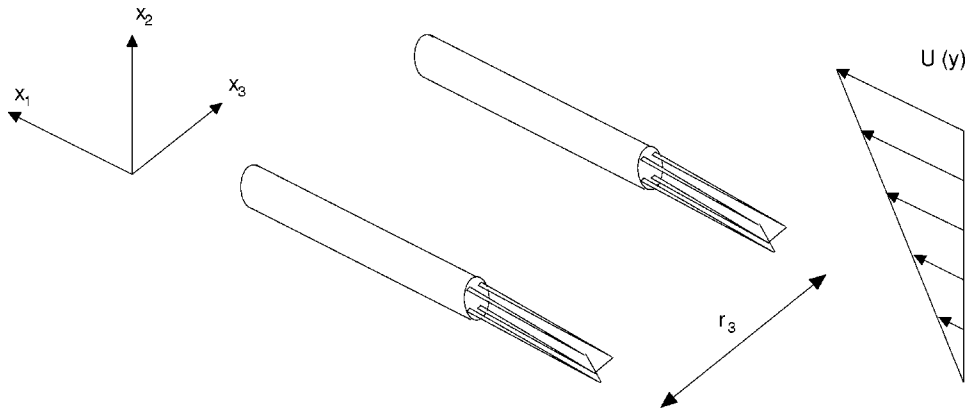

FIG. 3. Schematic of the measurement configuration: Each of the two X wires, separated in the transverse direction, $z=x_3$, detects two velocity components u and v (in the streamwise, $x=x_1$, and in the shear direction $y=x_2$, respectively). The separation between the two probes was measured by means of a charge-coupled device (CCD) camera with a high magnification lens and could be changed by means of a precision transverse gear from 0.8 mm to 70 mm.

TABLE III. List of observables with null contribution from the $j=0$ and 1 sectors.

n	Separation	Observable		
2	r_1	$S_{12}(r_1)$		
4	r_1	$S_{1112}(r_1)$	$S_{1222}(r_1)$	
6	r_1	$S_{111\,112}(r_1)$	$S_{111\,222}(r_1)$	$S_{122\,222}(r_1)$
2	r_3	$S_{12}(r_3)$		
4	r_3	$S_{1112}(r_3)$	$S_{1222}(r_3)$	
6	r_3	$S_{111\,112}(r_3)$	$S_{111\,222}(r_3)$	$S_{122\,222}(r_3)$

Clearly, using this procedure, systematic, uncontrolled errors are introduced by neglecting the higher j sectors. Similar considerations can be extended to tensorial correlation functions of any order. For example, Table III lists several observables which, according to the previous discussion and the symmetries of the experimental setup sketched in Fig. 3, do not present contributions from both sectors $j=0$ and $j=1$. In the table, the suffixes 1, 2, and 3 correspond to direction $x_1=x$, $x_2=y$, and $x_3=z$, respectively. The objects reported in the first three lines depend on the streamwise separation r_1 and can be evaluated by using a single X-wire probe and Taylor hypothesis. Those on the last three lines depend on the transverse separation r_3 and can be measured only by using at least two X-wire probes. Hereafter we mainly present results based on the two-probe approach.

Considering the schematic in Fig. 3, the two-point measurements consist of the acquisition of u and v at two points separated in direction z (see caption). On the other hand, for example, the single point measurement of $S_{1112}(r_1)$ with $u_1=u$ and $u_2=v$, as a function of time yields

$$S_{1112}(r_1) = \langle [u(t+r_1/U) - u(t)]^3 [v(t+r_1/U) - v(t)] \rangle. \quad (3)$$

This approach has been used, e.g., in Ref. 4 in the context of the homogeneous shear flow and in Ref. 11 at a single location in the atmospheric boundary layer to address the scaling properties of the $j=2$ sector. In Ref. 12, two single component wires, at fixed separation in the transverse direction z, are used in connection with the Taylor hypothesis to extract the scaling exponent of the $j=2$ sector, while a similar procedure with two X wires separated in the shear direction y permits investigation of the scaling behavior of the $j=1$ sector.

The purpose of the present work is to bypass the use of Taylor hypothesis by using the configuration described in Fig. 3. This allows us to compute the anisotropic observables depending on r_3 (Table III) by continuously changing the transverse separation between the two probes.

A. The homogeneous shear flow

The global parameters characterizing the homogeneous shear flow are summarized in Table I. In order to allow for direct comparison between data for the homogeneous shear flow and for the boundary layer—to be presented in Sec. III B—a common normalization procedure is used. For the homogeneous shear the relevant characteristic velocity is defined as

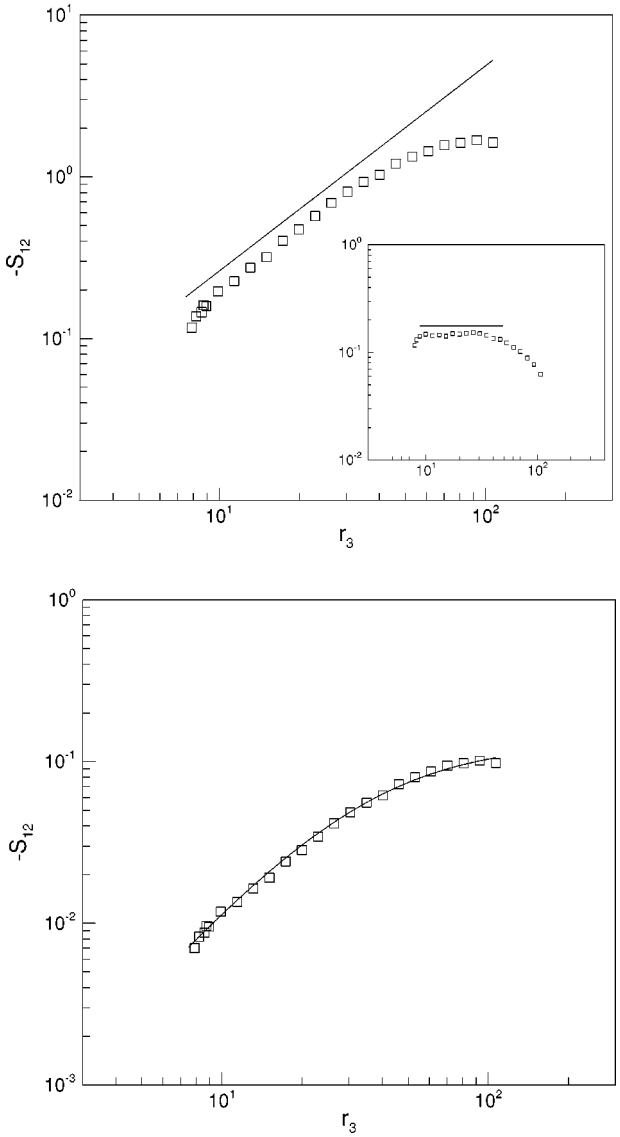

FIG. 4. Homogeneous shear flow. Top: Log-log plot of the mixed structure function of second order, $-S_{12}$ plotted as a function of the transverse separation r_3. All quantities are normalized with respect to the inner scaling defined by $u_\tau=\sqrt{\tau/\rho}$ and ν/u_τ. The solid line corresponds to the slope 1.22. The minimal length scale resolved is of the order of the dissipative scale. In the inset the same data are shown in compensated form, $-S_{12}/r_3^{1.22}$. Bottom: The same data are fitted by means of the expression given in Eq. (5), with $A_2=0.018$, $B_2=0.062$, and $D_2=3.27$, solid line.

$$u_\tau = \sqrt{\tau/\rho}, \quad (4)$$

where $\tau=\nu S-\langle uv\rangle$ with $S=dU/dy$ the mean shear.

In Fig. 4, the second order mixed structure function $S_{12}(r_3)$ is plotted as a function of the transverse separation. In addition to the r^2 behavior at smaller scales and to the large scale saturation, a distinct power law at intermediate scales emerges, allowing us to measure the scaling exponent $\xi_2(2)$ with good accuracy. The estimate $\xi_2(2)=1.22\pm0.07$ is indicated by the solid line, while the horizontal plateau in the inset, displaying the structure function in compensated form, shows the extension of the scaling region.

The same data have also been fitted by means of the expression proposed in Ref. 11 to model the behavior of a

generic structure function in the entire range of scales (bottom panel, solid line). In our case, the interpolation function for $S_{12}(r_3)$ is given by

$$S_{12}(r_3) = \frac{A_2 r_3^2 [1 + D_2(r_3/\ell_T)]^{-\xi_2(2)}}{[1 + B_2(r_3/\eta)^2]^{1-[\xi_2(2)]/2}} \tag{5}$$

and describes the superposition of a scaling behavior with coefficient $\xi_2(2)$ at intermediate scales, a large-scale saturation and a dissipative closure at small scales. Here, the exponent $\xi_2(2)$ is fixed by the direct fit estimated from the compensated plot in the top panel of Fig. 4, the transverse integral scale ℓ_T is evaluated according to its definition given in Table I, while A_2, B_2, and D_2 are the only fitting constants. The ability of Eq. (5) to correctly reproduce the experimental data can be appreciated by looking at the excellent agreement between the solid curve and the open symbols in the bottom panel of Fig. 4. Such a fitting procedure, not strictly necessary here, turns out to be useful later in the context of the TBL flow, hence a few more comments are appropriate. Physical considerations suggest an "inertia-dominated range" at intermediate separations. This range becomes shorter and shorter as the local Reynolds number decreases. Due to this reason, as one approaches the wall in a TBL, the contamination of viscous subrange and integral scale effects are unavoidable. The expression (5) must be seen as the simplest way to incorporate both effects.

Results concerning higher-order statistics of anisotropic fluctuations are shown in Fig. 5. In the top panel, the two transverse observables of order 4, namely, $S_{1112}(r_3)$ and $S_{1222}(r_3)$ are shown, both in their standard and compensated forms. A best fit yields for the exponent $\xi_2(4)$ a value of 1.7 ± 0.1, indicated by the solid line. The associated error accounts for both the deviation from a pure scaling law and for the slightly different behavior of $S_{1112}(r_3)$ with respect to $S_{1222}(r_3)$. The corresponding compensated structure functions of order 4 are shown in the inset of the top panel. Mixed structure functions of order 6 are displayed in the bottom panel of Fig. 5. In particular, with the configuration of Fig. 3, three transverse observables can be measured, namely, $S_{111\,112}(r_3)$, $S_{111\,222}(r_3)$, and $S_{122\,222}(r_3)$. Only the first two, with the best statistical properties, are shown in the figure. Here again, minimal differences in the scaling behavior of these quantities are observed. Typically, lower values of the exponents are achieved for structure functions with largest weight on the vertical velocity component, i.e., for the sixth order $S_{122\,222}$. The exponents increase with increasing weight of u, i.e., for the sixth order moving from $S_{122\,222}$ through $S_{111\,222}$ to $S_{111\,112}$. However, we find that a unique value of $\xi_2(6) = 2.05 \pm 0.15$ is able to fit satisfactorily the set of statistics of order 6. Previous experimental studies in both the atmospheric boundary layer and homogeneous shear flows[4,11] quoted values for the scaling exponents ranging from 1.05 to 1.3 for $\xi_2(2)$, from 1.42 to 1.56 for $\xi_2(4)$, and from 1.71 to 2.14 for $\xi_2(6)$. Each of these measurements is affected by an error bar of the order of 10% due to the choice of the range of scales fitted. Our findings are, therefore, consistent with all the other experimental measurements. The result for $\xi_2(2)$ is also close to the value 1.36 obtained with an analytical estimate based on a perturbative expansion on the anisotropy intensity.[23]

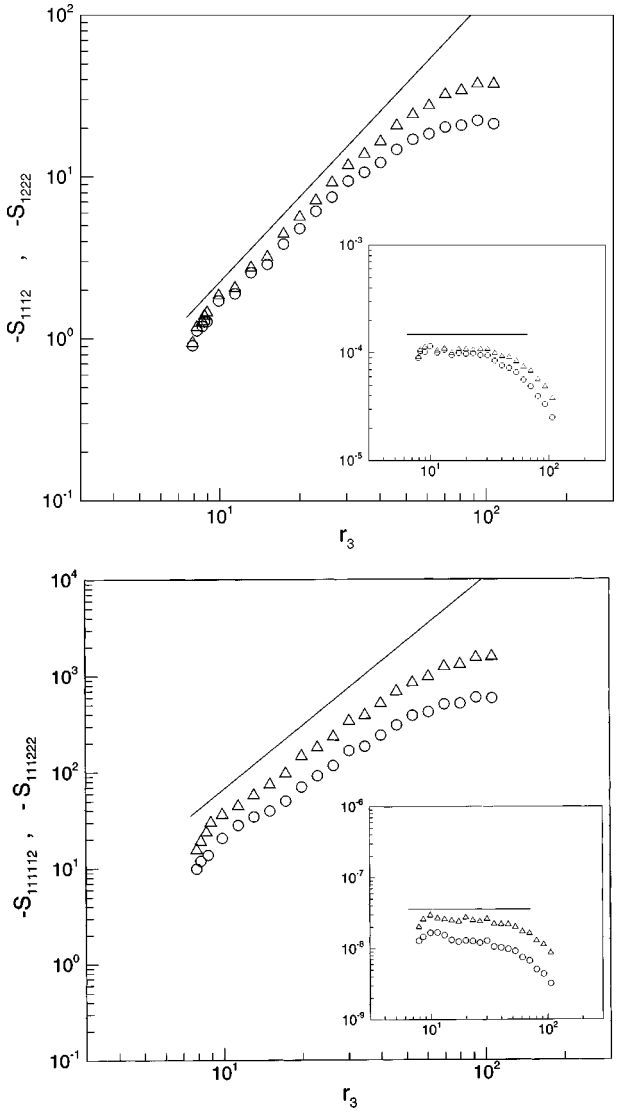

FIG. 5. Homogeneous shear flow. Top panel: The purely anisotropic mixed structure functions of order 4, S_{1112} (triangles) and S_{1222} (circles). The solid line indicates the slope of 1.7. In the inset the same data are compensated with $r^{1.7}$, same symbols. Bottom plot: Two purely anisotropic mixed structure functions of order 6, $S_{111\,112}$ (triangles) and $S_{111\,222}$ (circles). The solid line indicates the slope of 2.05. In the inset the same data are compensated with $r^{2.05}$, same symbols.

B. The turbulent boundary layer

To address the effect of shear intensity and different boundary conditions, we consider the more complex environment represented by the near-wall region of a fully developed turbulent boundary layer. In this flow configuration two basic difficulties emerge. The first one is associated with the thinness of the region where significant changes of the mean gradient occur, which poses severe restrictions on the probe dimensions. The second problem is related to the relatively large fluctuation level in the lower part of the log-region, which may cause troubles with Taylor hypothesis. Concern-

ing the first issue, a boundary layer as thick as possible was realized in a relatively large, yet well-controlled, experimental facility, as described in Sec. II. Moreover, to ensure a sufficient probe resolution, the measurements were limited to the log-region, sufficiently far from the boundary. The second point was instead entirely bypassed by addressing anisotropic observables depending only on the transverse separation r_3, as already explained for the HS configuration. Also in this case, the data we discuss are presented in dimensionless form, using the friction velocity

$$u_\tau = \sqrt{\tau_w/\rho} \tag{6}$$

as characteristic velocity scale, where τ_w is the average shear stress at the wall (Sec. II). This corresponds directly to the normalization used in Sec. III A, since in the near-wall region the total shear stress τ is constant in the wall-normal direction. The main issue is connected with the assessment of the anisotropic properties with changing distance from the wall.

In Fig. 6 we summarize the results for the fully anisotropic transverse structure functions already introduced in the previous section. The three panels show, from top to bottom, the observables of order 2, 4 and 6, respectively, while the different symbols correspond to different distances from the wall, from $y^+=350$ down to $y^+=90$. As one can see, the scaling properties are not as clear as in the HS case. Independently of the order of the structure function, farther from the wall a distinct scaling range emerges. As the wall is approached, the scaling behavior is less evident and a tendency towards saturation at large scales is observed. Here, in order to extract quantitative results one needs to consider also large scale effects. We generalized, therefore, the expression (5) to all orders, for separations much larger than the Kolmogorov scale

$$S_{\alpha_1 \ldots \alpha_n}(r_3) = A_n(y^+) r_3^{\xi_2(n)} \left[1 + D_n(y^+) \frac{r_3}{\ell_T} \right]^{-\xi_2(n)}. \tag{7}$$

By comparing the fit with the raw data, it is quite clear that the poor scaling closer to the wall is substantially explained in terms of saturation occurring earlier and earlier as the wall is approached. The inset in the top panel describes the fitting procedure and highlights the scaling law by removing the effect of the large scale saturation. The inset of the middle panel shows the anisotropic flatness, $-S_{1122}/S_{12}^2$, which highlights the high degree of intermittency shown by anisotropic fluctuations, independently of the distance from the wall. It is important to stress here that the good agreement with the data for all distances is obtained by fixing the scaling exponents $\xi_2(n)$ to the value obtained in the HS case for all orders, n; only the prefactors need to be changed with varying wall distance.

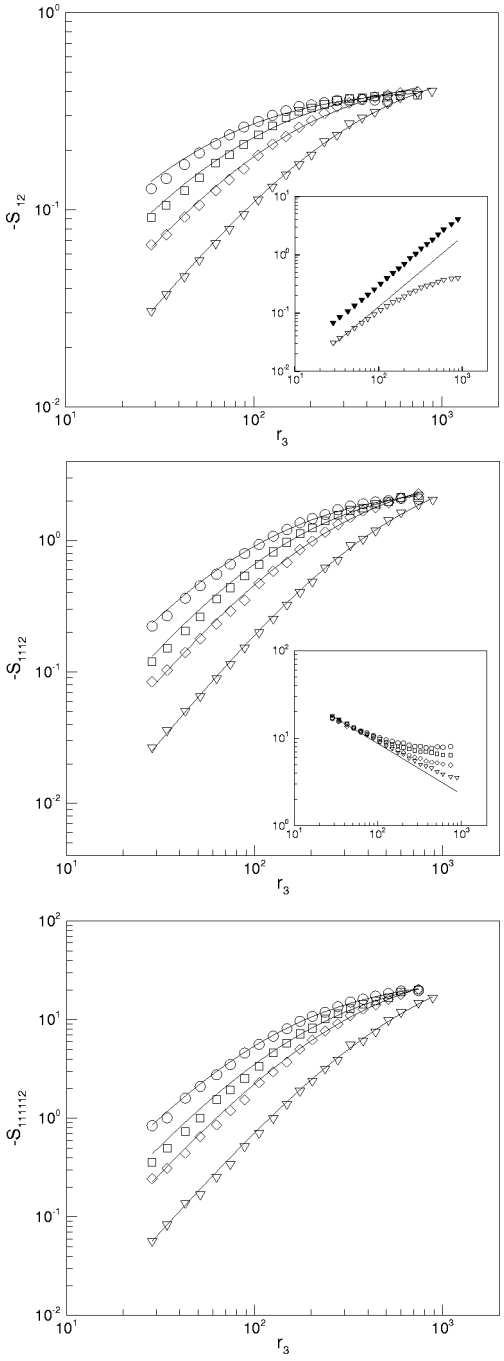

FIG. 6. Turbulent boundary layer: Log-log plot of the mixed structure functions vs transverse separation r_3 at different wall distances $y^+=350$ (triangles), 240 (diamonds), 140 (squares), 90 (circles), and for different orders $n=2$, 4, 6. In the top panel we show $-S_{12}$ (second order) where the corresponding solid lines represent the fit (7) keeping fixed $\xi_2(2)=1.22$ at varying A_2, D_2. The inset shows $-S_{12}$ in raw form (open triangles) and after compensation with saturation and viscous contributions (filled triangles) at $y^+=350$. The solid line indicates the slope 1.22. In the middle panel we show $-S_{1112}$ (fourth order), with $\xi_2(4)=1.7$ at varying A_4, D_4. In the inset we show the anisotropic flatness $-S_{1112}/S_{12}^2$ at corresponding locations. The solid line indicates the slope –0.65. In the bottom panel we show $-S_{111\,112}$ (sixth order) with $\xi_2(6)=2.05$ at varying A_6, D_6.

IV. CONCLUDING REMARKS

In this paper we have performed a systematic analysis of small-scale anisotropic turbulent properties in two different experimental setups, a homogeneous shear flow and a turbulent boundary layer. We have used two cross-wire probes to extract the leading anisotropic fluctuations of two-point correlation functions in the homogeneous directions without using the Taylor hypothesis. We have analyzed structure functions up to order $n=6$ finding a good agreement in the anisotropic exponents for all the different experimental con-

ditions we have considered. We compared the anisotropic properties by changing the normalized shear intensity, S^*, by a factor 2 and more. It is worth stressing that the Reynolds number of the present investigation is limited to relatively low values, of the order of 200. The conclusions we reach confirm previous results obtained at significantly higher Reynolds numbers and suggest that the behavior of the leading anisotropic sector is a robust feature of shear dominated turbulence.

The cleanest data are obtained for the homogeneous shear flow where a fit of the power law behavior allowed for a direct measurement of the anisotropic properties. In the turbulent boundary layer, we had to take into account also large scale saturation effects, especially close to the wall, in order to obtain a global fit of the structure functions behavior for all value of y^+. Our results support the exponent-only scenario of universality also in the anisotropic sector. In other words, we have been able to fit all experimental data by keeping fixed the scaling properties and adjusting only the prefactors.

The main drawback of all actual experimental setups is the impossibility to exactly disentangle different anisotropic sectors among themselves. This implies that subleading contributions coming from a sector with higher j's could spoil the quantitative measurements. In particular, the systematic differences observed here and in other studies[4,11] between the scaling of anisotropic correlation functions of the same order but with different tensorial components as $S^{(6)}_{111\,222}(r)$ and $S^{(6)}_{111\,112}(r)$ may well be due to the effects of subleading contributions coming from the $j \geqslant 4$ sectors in the SO(3) expansion.

ACKNOWLEDGMENTS

The authors acknowledge useful discussions with R. Piva and S. Kurien. This research was supported by MIUR and the EU under the Grant No. HPRN-CT 2000-00162 "Non Ideal Turbulence." The authors thank B. Devenish for a careful reading of the manuscript.

[1] U. Frisch, *Turbulence: The Legacy of A.N. Kolmogorov* (Cambridge University Press, Cambridge, 1995).
[2] S. Garg and Z. Warhaft, "On the small scale structure of simple shear flow," Phys. Fluids **10**, 662 (1998).
[3] X. Shen and Z. Warhaft, "The anisotropy of the small scale structure in high Reynolds number ($R_\lambda \sim 1000$) turbulent shear flow," Phys. Fluids **12**, 2976 (2000).
[4] X. Shen and Z. Warhaft, "On the higher order mixed structure functions in laboratory shear flow," Phys. Fluids **14**, 2432 (2002).
[5] A. Pumir, "Turbulence in homogeneous shear flows," Phys. Fluids **8**, 3112 (1996).
[6] L. Biferale and F. Toschi, "Anisotropic homogeneous turbulence: Hierarchy and intermittency of scaling exponents in the anisotropic sectors," Phys. Rev. Lett. **86**, 4831 (2001).
[7] L. Biferale and M. Vergassola, "Isotropy vs anisotropy in small-scale turbulence," Phys. Fluids **13**, 2139 (2001).
[8] I. Arad, V. L'vov, and I. Procaccia, "Correlation functions in isotropic and anisotropic turbulence: The role of the symmetry group," Phys. Rev. E **59**, 6753 (1999).
[9] I. Arad, L. Biferale, I. Mazzitelli, and I. Procaccia, "Disentangling scaling properties in anisotropic and inhomogeneous turbulence," Phys. Rev. Lett. **82**, 5040 (1999).
[10] I. Arad, B. Dhruva, S. Kurien, V. S. L'vov, I. Procaccia, and K. R. Sreenivasan, "Extraction of anisotropic contributions in turbulent flows," Phys. Rev. Lett. **81**, 5330 (1998).
[11] S. Kurien and K. R. Sreenivasan, "Anisotropic scaling contributions to high-order structure functions in high-Reynolds-number turbulence," Phys. Rev. E **62**, 2206 (2000).
[12] S. Kurien, V. L'vov, I. Procaccia, and K. Sreenivasan, "Scaling structure of the velocity statistics in atmospheric boundary layers," Phys. Rev. E **61**, 407 (2000).
[13] L. Biferale, I. Daumont, A. Lanotte, and F. Toschi, "Anomalous and dimensional scaling in anisotropic turbulence," Phys. Rev. E **66**, 056306 (2002).
[14] L. Biferale, G. Boffetta, A. Celani, A. Lanotte, F. Toschi, and M. Vergassola, "The decay of homogeneous anisotropic turbulence," Phys. Fluids **15**, 2105 (2003).
[15] A. Arneodo, C. Baudet, F. Belin, R. Benzi, B. Castaing, B. Chabaud, R. Chavarria, S. Ciliberto, R. Camussi, F. Chilla, B. Dubrulle, Y. Gagne, B. Hebral, J. Herweijer, M. Marchand, J. Maurer, J. F. Muzy, A. Naert, A. Noullez, J. Peinke, F. Roux, P. Tabeling, W. van de Water, and H. Willaime, "Structure functions in turbulence, in various flow configurations, at Reynolds number between 30 and 5000, using extended self-similarity," Europhys. Lett. **34**, 411 (1996).
[16] A. Staicu, B. Vorselaars, and W. van de Water, "Turbulence anisotropy and the SO(3) description," Phys. Rev. E **68**, 046303 (2003).
[17] L. Biferale, E. Calzavarini, F. Toschi, and R. Tripiccione, "Universality of anisotropic fluctuations from numerical simulations of turbulent flows," Europhys. Lett. **64**, 461 (2003).
[18] L. Biferale, D. Lohse, I. M. Mazzitelli, and F. Toschi, "Probing structures in channel flow through SO(3) and SO(2) decomposition," J. Fluid Mech. **452**, 39 (2002).
[19] F. H. Champagne, V. G. Harris, and S. Corrsin, "Experiments in nearly homogeneous turbulent shear flows," J. Fluid Mech. **41**, 81 (1970).
[20] S. Tavoularis and S. Corrsin, "Experiments in nearly homogeneous turbulent shear flow with a uniform mean temperature gradient. Part 1," J. Fluid Mech. **104**, 311 (1981); "Experiments in nearly homogeneous turbulent shear flow with a uniform mean temperature gradient. Part 2. The fine structure," *ibid*. **104**, 349 (1981).
[21] S. Cerutti and Ch. Meneveau, "Statistics of filtered velocity in grid and wake turbulence," Phys. Fluids **12**, 1143 (2000).
[22] J. L. Lumley, "Interpretation of time spectra measured in high-intensity shear flows," Phys. Fluids **8**, 1056 (1965).
[23] V. S. L'vov, I. Procaccia, and V. Tiberkevich, "Scaling exponents in anisotropic hydrodynamic turbulence," Phys. Rev. E **67**, 026312 (2003).